Vibrational effects on electron-impact valence excitations of SF_6

Noboru Watanabe,* Tsukasa Hirayama, and Masahiko Takahashi
Institute of Multidisciplinary Research for Advanced Materials, Tohoku University, Sendai 980-8577, Japan

(Received 28 April 2019; published 20 June 2019)

We report an angle-resolved electron-energy-loss spectroscopy study on the valence excitations of SF_6. Momentum-transfer-dependent generalized oscillator strengths (GOSs) or GOS profiles of the low-lying valence excitations have been derived from electron-energy-loss spectra measured at an incident electron energy of 3 keV. We have also performed theoretical calculations of the GOS profiles involving the influence of molecular vibration. Comparisons between experiment and theory have revealed that coupling between electronic states through molecular vibration plays a significant role in the $1\,^1T_{1g}$ dipole-forbidden transition.

DOI: 10.1103/PhysRevA.99.062708

I. INTRODUCTION

Sulfur hexafluoride (SF_6) has been widely used as an insulating medium in electric power technology and also for dry plasma etching in the semiconductor industry. Interactions of electrons with SF_6 have thus received considerable interest [1,2]. Besides, electron- and photon-induced electron excitations of this molecule are of interest from the viewpoint of molecular spectroscopy; a high potential barrier created by the constituent F atoms leads to the unusual electron excitation spectra of SF_6 [3–5].

Owing to the practical and fundamental importance, various investigations have been carried out for the valence excitations of SF_6 [1,5–12]. For instance, optical oscillator strengths have been determined for the molecule by means of photoabsorption and electron-scattering techniques. To make assignments of the observed spectral features, improved virtual orbital calculations were performed by Hay [13] and the results were used to interpret the electron scattering measurements by Trajmar and Churjian [11]. Later, Sze and Brion [12] proposed another plausible assignment using the term values derived from inner-shell excitations. Although there are some controversies in the proposed assignments, the studies have consistently shown that the lowest excited state arises from promotion of an electron from the $1t_{1g}$ nonbonding orbital to the $6a_{1g}$ antibonding orbital, and further revealed that several dipole-forbidden bands, including the $1t_{1g} \rightarrow 6a_{1g}$ excitation, appear in the photoabsorption spectrum. Appearance of a dipole-forbidden band in an absorption spectrum has generally been explained by the influence of molecular vibration. Coupling between electronic states through molecular vibration, known as Herzberg-Teller vibronic coupling mechanism, changes the nature of the forbidden transition [14]. Thus, to get a full understanding of the valence excitations in SF_6, detailed knowledge of the vibrational effects is needed.

High-energy angle-resolved electron-energy-loss spectroscopy (EELS) provides a powerful means to investigate such vibrational effects. The electron-scattering cross section is proportional to the so-called generalized oscillator strength (GOS), which is related to the Fourier transform of the overlap between the wave functions of the initial and final target states [15,16]. Since the GOS for transition to each excited state exhibits its own characteristic momentum-transfer dependence, a close examination of the GOS profile allows one to see how electronic states are coupled to each other through molecular vibration. Based on this principle we have investigated the influence of molecular vibration on valence excitations of CF_4 [17], CO_2 [18], and N_2O [19].

For SF_6 an angle-resolved EELS study was reported by Ying *et al.* [20]. In the study, the GOS was determined as a functions of electron energy loss and momentum transfer, and tentative assignments of the valence excitations were made based on the momentum-transfer dependence of the transition probabilities. EELS measurements on SF_6 were performed also by Rocco *et al.* [21] and GOS profiles were obtained for low-lying transitions. To our knowledge, however, no attempt has been made to examine the vibrational effects on the valence excitations of SF_6 using the EELS technique.

In this paper we report an angle-resolved EELS study on SF_6. The main purpose of the study is to improve the knowledge of the valence excitations of the molecule. EELS measurements on SF_6 have been performed at an incident electron energy of 3 keV and GOS profiles have been obtained over a wide momentum-transfer region. Furthermore, we have carried out the theoretical calculation of GOS profiles at the level of the equation-of-motion coupled-cluster treatment. In the calculation vibrational effects have been taken into account. Comparisons between experiment and theory have revealed that the asymmetric SF stretching mode plays a crucial role in the $1t_{1g} \rightarrow 6a_{1g}$ excitation.

II. THEORETICAL BACKGROUND AND EXPERIMENT

Within the Born approximation, the double-differential scattering cross section is expressed as [15]

$$\frac{d^2\sigma}{d\Omega dE} = \frac{|\boldsymbol{k}_s|}{|\boldsymbol{k}_i|}\frac{2}{K^2E}\frac{df(K,E)}{dE}, \quad (1)$$

*noboru.watanabe.e2@tohoku.ac.jp

where $\boldsymbol{k}_\mathrm{i}$ and $\boldsymbol{k}_\mathrm{s}$ are the momenta of the incident and scattered electrons, respectively, $K(=|\boldsymbol{k}_\mathrm{i}-\boldsymbol{k}_\mathrm{s}|)$ denotes the momentum transfer, and E the electron energy loss. The cross section is proportional to the differential GOS

$$\frac{df(K,E)}{dE}=\frac{1}{4\pi}\int d\Omega_{\boldsymbol{K}}\frac{2E}{K^2}\sum_n\left|\langle\Phi_n|\sum_j\exp\left(i\boldsymbol{K}\cdot\boldsymbol{r}_j\right)|\Phi_0\rangle\right|^2\times\delta(E-E_{n0}). \tag{2}$$

Here Φ_0 and Φ_n represent the wave functions of the initial and final target states, E_{n0} is the energy difference between these states, and $\boldsymbol{r}_j$ the position of the jth electron. To account for the random orientation of gaseous target molecules, the differential GOS is spherically averaged. It should be noted that at $K=0$, the GOS becomes equal to the optical oscillator strength (OOS)

$$\lim_{K\to0}\frac{df(\boldsymbol{K},E)}{dE}=2E\sum_n\left|\langle\Phi_n|\sum_j\hat{\boldsymbol{K}}\cdot\boldsymbol{r}_j|\Phi_0\rangle\right|^2\delta(E-E_{n0}), \tag{3}$$

with $\hat{\boldsymbol{K}}$ being $\boldsymbol{K}/K$, and under the condition the electron-scattering cross section is proportional to the photoabsorption cross section.

The EELS spectrometer used in this study has been described in detail elsewhere [22]. Briefly, it consists of an electron gun, a molecular-beam source, and a hemispherical electron analyzer equipped with a retarding lens system. The electron analyzer is mounted on a turntable to adjust the scattering angle. Rotation of the turntable is accomplished by turning a high-precision worm gear with a 720:1 ratio. A collimated electron beam is crossed at right angle with an effusive molecular beam from a nozzle with an inner diameter of 0.5 mm. The electrons scattered at a particular angle θ with respect to the incident electron-beam direction are decelerated by the retarding lens and then energy analyzed using the hemispherical analyzer, which is operated at pass energy of 80 eV. Electron-energy-loss spectra have been measured by scanning a deceleration voltage applied to the retarding lens.

EELS experiments on SF_6 were carried out at an incident electron energy of $E_0=3.0$ keV for a series of scattering angles from 1.7° to 7.2°. The instrumental energy resolution was $1.1\sim1.2$ eV full width at half maximum. In the measurements high-grade SF_6 gas (>99.999%) delivered by Japan Fine Products was used without further purification. The electron-energy-loss spectra were recorded at two different ambient sample gas pressures, $\sim1.0\times10^{-4}$ and $\sim0.4\times10^{-5}$ Pa, to remove contributions from background signals by taking the difference between them.

The EELS spectra were converted to the GOS distributions on a relative scale using Eq. (1) and put on an absolute scale by means of the Bethe sum rule [16]:

$$\int\frac{df(K,E)}{dE}dE=N, \tag{4}$$

where N is the total number of electrons in the target. In the normalization procedure the intensity of the relative GOS distribution obtained at each scattering angle was integrated over E ranges up to 170 eV. Although the magnitude of the momentum transfer, $K=[{k_\mathrm{i}}^2+{k_\mathrm{s}}^2-2k_\mathrm{i}k_\mathrm{s}\cos\theta]^{1/2}$, varies with E for a fixed θ, it is effectively constant over the energy-loss region measured. The fraction of the valence shell GOS above the upper limit of the integration region was estimated by integration of a function A/E^B least square fitted to the experimental data. The sum of these integrated intensities was then normalized to $N=49.7$, which corresponds to the total number of valence electrons, 48, plus corrections for Pauli-excluded transitions from the inner shells to the already occupied valence orbitals [23].

III. THEORETICAL CALCULATION

Theoretical calculations were conducted for low-lying valence excitations of SF_6. Details of the theoretical method used are given elsewhere [17,18]. Briefly, the GOS of a transition from the v vibrational level in the initial electronic state 0 to the v' vibrational level in the excited electronic state n is expressed as

$$f_{0v\to nv'}(K)=\frac{1}{4\pi}\frac{2E_{nv',0v}}{K^2}\int d\Omega_{\boldsymbol{K}}|\langle\chi_{nv'}(\boldsymbol{Q})|\times\varepsilon_{n0}(\boldsymbol{K},\boldsymbol{Q})|\chi_{0v}(\boldsymbol{Q})\rangle|^2, \tag{5}$$

by assuming the Born-Oppenheimer approximation. Here χ_{0v} and $\chi_{nv'}$ are the vibrational wave functions of the initial and final target states, respectively, and $\boldsymbol{Q}$ denotes the normal vibrational coordinates. $E_{nv',0v}$ is the energy difference between these states and $\varepsilon_{\mathrm{n}0}(\boldsymbol{K},\boldsymbol{Q})$ denotes the electronic transition moment,

$$\varepsilon_{n0}(\boldsymbol{K},\boldsymbol{Q})=\langle\Psi_n(\boldsymbol{r}_1,\boldsymbol{r}_2,\ldots,\boldsymbol{r}_N;\boldsymbol{Q})|\sum_j\exp(i\boldsymbol{K}\cdot\boldsymbol{r}_j)\times|\Psi_0(\boldsymbol{r}_1,\boldsymbol{r}_2,\ldots,\boldsymbol{r}_N;\boldsymbol{Q})\rangle. \tag{6}$$

What we have measured in the present study is the total intensity of the whole band of the $0\to n$ electronic excitation and $f_{0v\to nv'}(K)$ is thus summed over all vibrational levels in the excited state n. Since energy separations between vibrational levels are generally much smaller than those between electronic states, it would be a good approximation to replace the excitation energies $E_{nv',0v}$ to a constant value $E_{n,0}$. With this approximation and by using the closure relation of the vibrational eigenstates, the following expression is obtained:

$$f_{0v\to n}(K)=\sum_{v'}f_{0v\to nv'}(K)=\frac{2E_{n,0}}{K^2}\int|\chi_{0v}(\boldsymbol{Q})|^2M_{n0}(K,\boldsymbol{Q})d\boldsymbol{Q}, \tag{7}$$

with

$$M_{n0}(K,\boldsymbol{Q})=\frac{1}{4\pi}\int|\varepsilon_{n0}(\boldsymbol{K},\boldsymbol{Q})|^2d\Omega_{\boldsymbol{K}}. \tag{8}$$

Here we describe $\chi_{0v}(\boldsymbol{Q})$ as a product of harmonic oscillator functions $\xi_{vL}(Q_L)$, with Q_L being the normal coordinate of the Lth vibrational mode and further assume that $M_{n0}(K,\boldsymbol{Q})$ changes slowly with $\boldsymbol{Q}$ in the vicinity of the equilibrium geometry of the initial electronic state, $\boldsymbol{Q}_0$. As a result, the following

TABLE I. Harmonic vibrational frequencies of SF_6 (cm^{-1}).

Mode	Symmetry	MP2	Expt. [30]
ν_1	a_{1g}	771.0	774.55
ν_2	e_g	646.3	643.35
ν_3	t_{1u}	952.9	947.98
ν_4	t_{1u}	605.8	615.02
ν_5	t_{2g}	514.8	523.56
ν_6	t_{2u}	342.1	348.08

computationally tractable expression is obtained [17]:

$$f_{0v\to n}(K) = \frac{2E_{n,0}}{K^2} M_{n0}(K, \boldsymbol{Q}_0) + \frac{2E_{n,\,0}}{K^2} \times \sum_L \langle \xi_{vL} | M_{n0}(K, \boldsymbol{Q}_0 + Q_L \hat{\boldsymbol{q}}_L) - M_{n0}(K, \boldsymbol{Q}_0) | \xi_{vL} \rangle, \tag{9}$$

where $\hat{\boldsymbol{q}}_{\rm L}$ denotes a unit vector that points along the Lth normal coordinate. The first term is equivalent to the GOS of the molecule at the equilibrium geometry and the second term represents the influence of molecular vibration. This method not only reduces the computational cost, compared to the calculation over the full $\boldsymbol{Q}$ space according to Eq. (7), but also allows us to discuss vibrational effects in detail by dividing those into contributions from each normal mode. A similar method has also been used to infer the influence of molecular vibration on electron momentum density distributions of various molecules [24–26].

In this study two kinds of theoretical calculations were carried out. One is the calculation for SF_6 whose nuclear positions are fixed at the equilibrium geometry (equilibrium geometry calculation) and the other is that involving vibrational effects based on Eq. (9) (vibrational effects calculation). For making the calculations, geometry optimization and a normal-mode analysis were carried out using the second-order Møller-Plesset (MP2) method. The augmented correlation-consistent polarization valence triple-zeta (aug-cc-pVTZ) basis [27,28] was used, while f-type diffuse functions were excluded to save computational time. The vibrational frequencies obtained by means of the General Atomic Molecular Electronic Structure System (GAMESS) program [29] are presented in Table I, together with experimental data reported in the literature [30]. The computed results show reasonable accordance with experiment. The theoretical SF bond length in the equilibrium geometry is 1.573 98 Å, being in good agreement with the experimental value, 1.564 ± 0.01 Å [1].

Subsequently, $M_{n0}(K,\boldsymbol{Q})$'s were computed at several molecular geometries distorted from the equilibrium along each normal coordinate. At each distorted geometry the electronic wave functions of SF_6 were calculated at the levels of the coupled-cluster singles and doubles (CCSD) and equation-of-motion CCSD (EOM-CCSD) treatments [31] for the ground and excited states, respectively. The core orbitals were kept doubly occupied in the calculations. The CCSD and EOM-CCSD methods have been known for their ability of accurate and well-balanced description of electronic states. In the calculations, we used basis sets of valence double-zeta quality, cc-pVDZ for F [27] and cc-pV(D+d)Z for S [32], augmented with two sets of s- and p-type diffuse functions. The Gaussian exponents of the s-type diffuse functions are 0.098 63 and 0.025 (0.0507 and 0.012 85); those of the p-type functions are 0.085 02 and 0.0208 (0.0399 and 0.009 76) for F (S) [28]. Besides, a d-type diffuse function with Gaussian exponent of 0.155 [32] was added for S. The evaluations of the transition matrix element and spherical averaging over the direction of $\boldsymbol{K}$ in Eq. (8) were performed analytically [33–35] and $f_{0v\to n}(K)$ was then calculated according to Eq. (9). Finally, the GOS was obtained by summing up $f_{0v\to n}(K)$ weighted by the Boltzmann distribution of the vibrational level, $P_v(T)$:

$$f_{0\to n}(K) = \sum_v P_v(T) f_{0v\to n}(K), \tag{10}$$

where T is temperature, being assumed to be 300 K in the calculation.

IV. RESULTS AND DISCUSSION

A. Electron-energy-loss spectra

SF_6 is an octahedral molecule belonging to the O_h point group and its electronic configuration can be written as

$$(\text{core})^{22}(4a_{1g})^2(3t_{1u})^6(2e_g)^4(5a_{1g})^2(4t_{1u})^6(1t_{2g})^6(3e_g)^4 \times \{(5t_{1u})^6(1t_{2u})^6\}(1t_{1g})^6(6a_{1g})^0(6t_{1u})^0,$$

where the $5t_{1u}$ and $1t_{2u}$ orbitals are almost degenerate in energy. For the molecule in the ground state, only transitions to $^1T_{1u}$ states are dipole allowed. The excitation energies calculated by the EOM-CCSD method are presented in Table II, together with available experimental data [11,12] as well as the single-excitation configuration-interaction (SECI) calculation with 6-311 + G(d) basis by Winstead and McKoy [36]. The SECI approach is the simplest *ab initio* method for calculations of excitation energies, in which the wave functions are constructed from singly excited determinants. To assess the theoretical-model dependence, a time-dependent density-functional theory (TDDFT) calculation [37] was also carried out using the M06-2X functional, which has been shown to give reasonable excitation energies for both valence and Rydberg transitions of simple molecules [38]. As can be seen from Table II, the EOM-CCSD calculation shows excellent agreement with experiment, while the TDDFT calculation underestimates the excitation energies. On the other hand, the SECI calculation significantly overestimates the experiments. The results indicate that accurate treatment of electron correlation is required to well account for the experimental results.

Based on the EOM-CCSD calculation, we discuss the assignment of the spectral features of SF_6. Below 12 eV, two broad features have been observed at $E \sim 9.8$ and 11.5 eV, which can unambiguously be attributed to the $1\,^1T_{1g}$ and $1\,^1T_{1u} + 1\,^1T_{2u}$ transitions, respectively. Above 12 eV, the EOM-CCSD calculation has predicted the existence of the $2\,^1T_{1g}$ dipole-forbidden band at ~12.8 eV, being consistent with experimental observations [11,12], and also shown that a band observed at ~13.3 eV may be associated with the $2\,^1T_{2u} \sim 1\,^1A_{1u}$ states arising from the $1t_{1g} \to 6t_{1u}$, $3e_g \to 6a_{1g}$, and $1t_{2g} \to 6a_{1g}$ excitations.

On the basis of the above assignment we have analyzed our experimental data. Figure 1 shows the electron-energy-loss

TABLE II. Excitation energies of SF_6 (eV).

		Theoretical			Experimental	
State	Character	EOM-CCSD[a]	TDDFT	SECI [36]	EELS [11]	Dipole EELS [12]
$1\,^1T_{1g}$	$1t_{1g} \rightarrow 6a_{1g}$	9.969	9.32	12.17	9.8	9.596
$1\,^1T_{2u}$	$1t_{2u} \rightarrow 6a_{1g}$	11.067	10.36	13.19	11.0	10.98–12.27
$1\,^1T_{1u}$	$5t_{1u} \rightarrow 6a_{1g}$	11.441	10.72	13.45	11.6	
$2\,^1T_{1g}$	$1t_{1g} \rightarrow 7a_{1g}$	12.842	12.56		12.8	12.38–12.69
$2\,^1T_{2u}$	$1t_{1g} \rightarrow 6t_{1u}$	13.235	12.98		13.3	13.14–13.31
$2\,^1T_{1u}$	$1t_{1g} \rightarrow 6t_{1u}$	13.268	13.03			
$1\,^1E_g$	$3e_g \rightarrow 6a_{1g}$	13.358	12.70			
$1\,^1T_{2g}$	$1t_{2g} \rightarrow 6a_{1g}$	13.409	12.65			
$1\,^1E_u$	$1t_{1g} \rightarrow 6t_{1u}$	13.524	13.21			
$1\,A_{1u}$	$1t_{1g} \rightarrow 6t_{1u}$	13.526	13.19			

[a]Vertical excitation energies for equal SF bond distances of $R_{SF} = 1.573\,98$ Å; all energies relative to the energy of the $X\,^1A_{1g}$ ground state at the CCSD level: $E(\mathrm{CCSD}) = -995.403\,69$ hartree.

spectra at representative scattering angles. The spectra are presented in the form of the differential GOS distributions. To highlight contributions of the valence excitations, expanded views of the low-E region are depicted in Fig. 2 for $\theta = 1.7°$, 3.7°, and 6.2° ($K^2 = 0.18$, 0.89, and 2.53 a.u.). The scattering angles are selected so that the change in relative intensity of the transition bands can be recognized. Contributions of individual transitions were separated by using a deconvolution procedure which assumes a Gaussian curve for each transition band. The widths of the Gaussian curves were inferred from the instrumental energy resolution and the Franck-Condon widths obtained from the high-energy-resolution EELS studies [11,12], while the peak heights of the Gaussians were used as fitting parameters to reproduce the experimental data. The deconvoluted curves are shown as dashed lines and their sum as a solid line in Fig. 2. The fitting procedure was applied to a series of the energy-loss spectra at each scattering angle, and the GOS profiles of the $1\,^1T_{1g}$ and $1\,^1T_{1u} + 1\,^1T_{2u}$ transition bands were obtained by plotting the areas under the corresponding Gaussian curves against the momentum-transfer value.

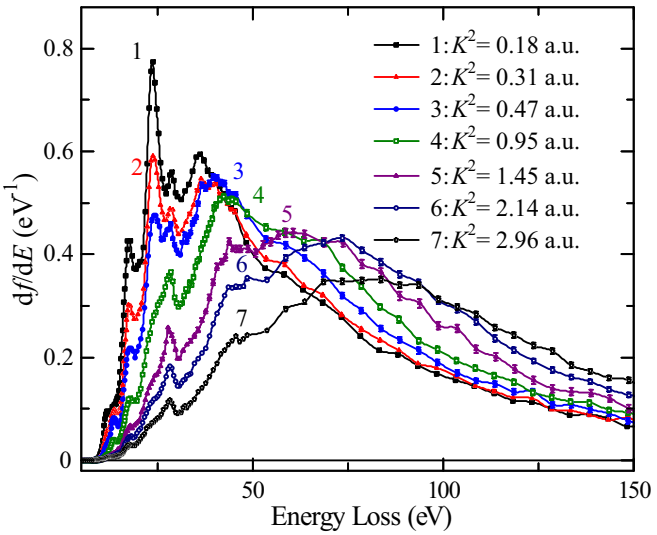

FIG. 1. Angle-resolved electron-energy-loss spectra of SF_6, which are presented in the form of the GOS distributions.

B. GOS profiles

Figure 3 shows the experimental GOS profile of the $1\,^1T_{1g}$ lowest-lying transition, which is ascribed to the excitation

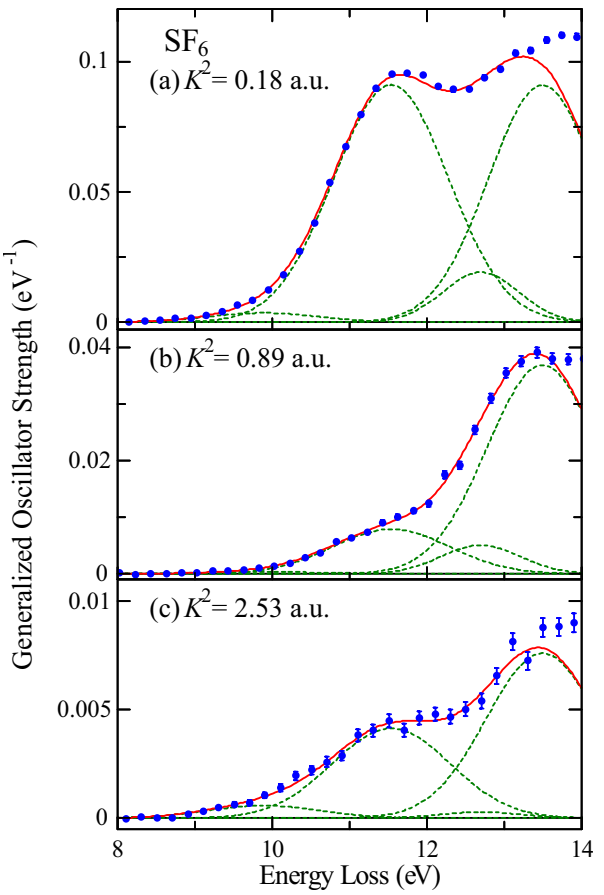

FIG. 2. Expanded view of the low-E region of the electron-energy-loss spectra at $\theta =$ (a) 1.7°, (b) 3.7°, and (c) 6.2°. The dotted curves are the deconvolution functions and the solid curve is their sum.

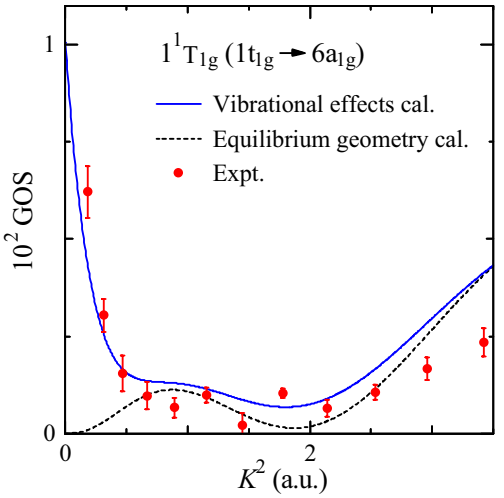

FIG. 3. Comparison between the experimental and theoretical GOS profiles of the $1\,^1T_{1g}$ transition. The solid and dashed lines represent the vibrational effects and equilibrium geometry calculations, respectively.

from the $1t_{1g}$ highest-occupied orbital to the $6a_{1g}$ unoccupied orbital. Also depicted in the figure are the equilibrium geometry calculation (dashed lines) and the vibrational effects calculation (solid lines). A comparison between experiment and theory shows that the equilibrium geometry calculation significantly underestimates the experiment below $K^2 = 0.5$ a.u. The calculation predicts zero intensity at $K^2 = 0$, where the GOS converges to the optical oscillator strength, while the experimental value increases with decreasing momentum transfer at small K^2 despite the dipole-forbidden nature of the $1\,^1T_{1g}$ transition. The observation cannot be explained if assuming the nuclear positions within the molecule are fixed at the equilibrium geometry, and it thus strongly suggests that the $1\,^1T_{1g}$ transition is substantially affected by molecular vibration. Indeed, the discrepancy from the experiment at small K^2 is mostly resolved by the inclusion of vibrational effects.

In Fig. 4 we show the experimental and theoretical GOS profiles of the second band at ∼11.5 eV, which is ascribed to the $1\,^1T_{2u}$ and $1\,^1T_{1u}$ transitions. Also depicted in the figure is the experimental result reported by Rocco *et al.* [21]. For ease of comparison, all data are multiplied by a factor of 10 above $K^2 = 0.7$ a.u. It can be seen from Fig. 4 that the two kinds of calculations are both in good accordance with the present experiment, suggesting a minor role of vibrational effects. The OOS obtained from the vibrational effects calculation is 0.403, being in reasonable agreement with the reported experimental value, 0.3828, for the associated energy region from 10.1 to 13.0 eV [39]. By contrast to our experimental result, the GOS values measured by Rocco *et al.* are considerably lower than the theoretical prediction below $K^2 \sim 0.7$ a.u. The origin of the differences is not clear now but it may, at least partly, come from low statistical accuracy of their electron-energy-loss spectra. To get a further insight into the 11.5-eV band, the theoretical GOS profiles of the $1\,^1T_{2u}$ and $1\,^1T_{1u}$ transitions are separately presented in the right-hand panels of Fig. 4. The vibrational effects calculation predicts appreciable influences of molecular vibration on these transitions at small momentum transfer. However, the

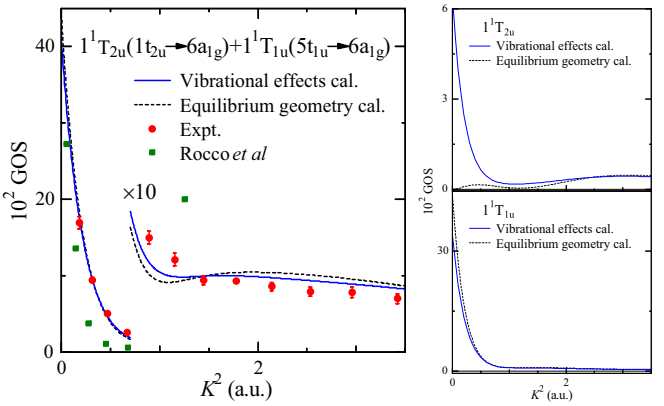

FIG. 4. Comparison between the experimental and theoretical $\{1\,^1T_{2u} + 1\,^1T_{1u}\}$ GOS profiles. The solid and dashed lines represent the vibrational effects and equilibrium geometry calculations, respectively. Also depicted in the figure is the experimental result by Rocco *et al.* [21]. For ease of comparison all data are multiplied by a factor of 10 above $K^2 = 0.7$ a.u. The right-hand-side panels separately present the theoretical GOS profiles of the $1\,^1T_{2u}$ and $1\,^1T_{1u}$ transitions.

vibrational effects are mostly canceled out when the two GOS profiles are summed up.

The theoretical calculations have been performed also for the $2\,^1T_{1g}$ transition at ∼12.8 eV. Owing to the rather small energy separations from close-lying transitions, the contribution of the 12.8-eV band could not be extracted from the present measurements, and hence, only theoretical results are presented in Fig. 5. It can be seen from the figure that the intensity of the equilibrium geometry calculation vanishes at zero momentum transfer, as expected for the $2\,^1T_{1g}$ transition being dipole forbidden. By contrast, the vibrational effects curve rises rapidly with the decrease in momentum transfer and has a maximum at $K^2 = 0$. The theoretical OOS value is 0.0117, being similar to that of the $1\,^1T_{1g}$ transition, 0.0101. It implies that the $2\,^1T_{1g}$ transition may appear in the

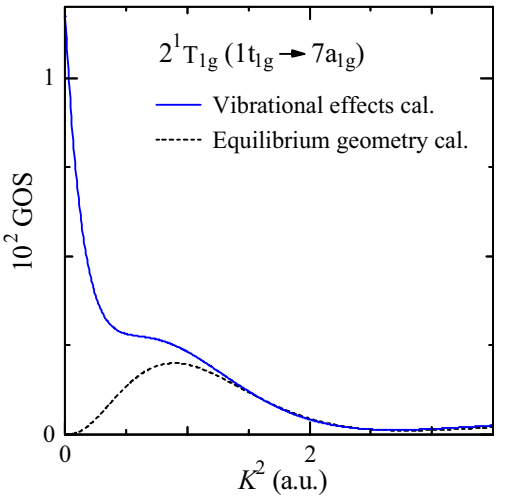

FIG. 5. Theoretical GOS profiles of the $2\,^1T_{1g}$ transition. The solid and dashed lines represent the vibrational effects and equilibrium geometry calculations, respectively.

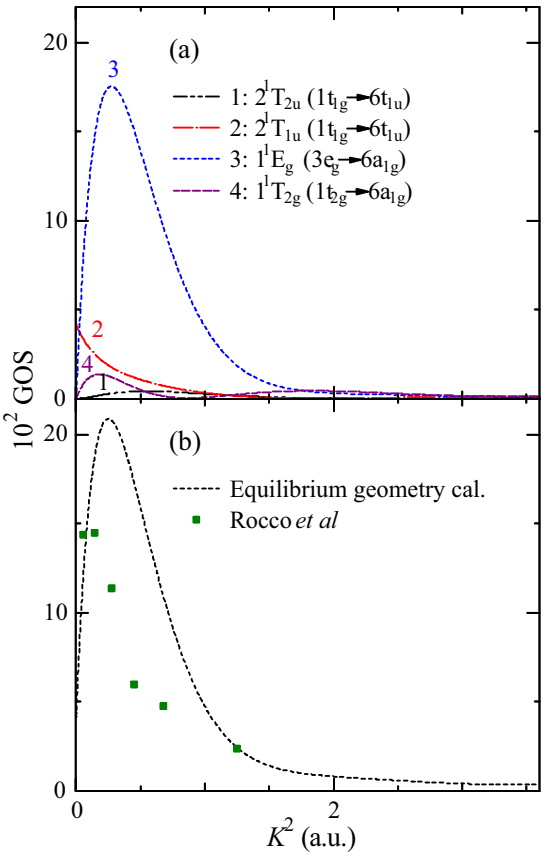

FIG. 6. (a) Equilibrium geometry calculations of the GOS profiles for the transitions associated with the 13.3-eV band and (b) a comparison of their sum with the experiment by Rocco *et al.* [21]. The results for the $1\,^1E_u$ and $1\,A_{1u}$ transitions are not presented here, because of their negligibly small intensities.

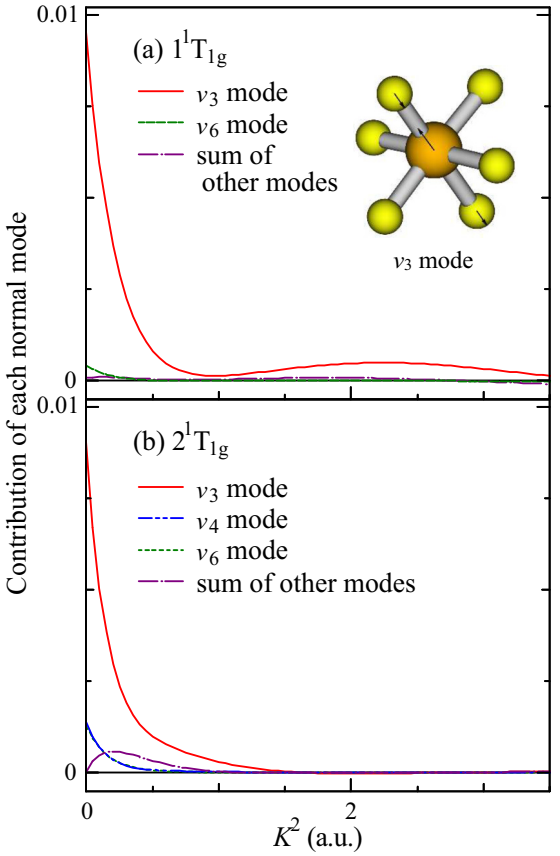

FIG. 7. Contributions of the individual vibrational modes to the GOS profiles of the (a) $1\,^1T_{1g}$ and (b) $2\,^1T_{1g}$ transitions. Inset in the figure is the pictorial representation of the v_3 mode. Since the contributions of the v_1, v_2, v_4, and v_5 modes to the $1\,^1T_{1g}$ transition are quite small, they are presented in the form of their sum. Similarly, the sum of the contributions of the v_1, v_2, and v_5 modes is depicted for the $2\,^1T_{1g}$ transition.

photoabsorption spectrum as a band whose intensity is comparable to that of the $1\,^1T_{1g}$ transition. Indeed, such a spectral feature has been observed at ∼12.8 eV in the OOS distribution reported by Sze and Brion [12].

We now turn our attention to the fourth band at ∼13.3 eV, which may be associated with several excited states (see Table II). The theoretical GOS profiles of the individual excitations are depicted in Fig. 6(a), and their sum is compared with the experiment by Rocco *et al.* [21] in Fig. 6(b). It should be noted that because of the limitation of our computational resource, only the equilibrium geometry calculations were performed for these transitions. As can be seen from Fig. 6(a), the $1\,^1E_g$ transition governs the intensity at $K^2 = 0.1 \sim 1.2$ a.u. It indicates that the 13.3-eV feature in the nondipole regime can be ascribed mainly to the $1\,^1E_g$ state, which arises from the $3e_g \rightarrow 6a_{1g}$ excitation. Inclusion of vibrational effects would not change this conclusion because of the dominant contribution from the $1\,^1E_g$ transition. Figure 6(b) shows that similar to the case for the 11.5-eV band, the theoretical calculation predicts a higher intensity than observed by Rocco *et al.* at $K^2 = 0.3 \sim 0.7$ a.u. The statistical errors in the EELS measurements and neglecting the vibrational effects in the present calculation are possible causes of the discrepancy between experiment and theory, and further studies are desired for the 13.3-eV band.

C. Contributions from each vibrational normal mode

According to our theoretical approach, the vibrational effects on a GOS profile can be divided into contributions from each normal mode. Figure 7 presents the results of such analysis for the $1\,^1T_{1g}$ and $2\,^1T_{1g}$ GOS profiles, where substantial vibrational effects have been observed. It is evident from the figure that the v_3 asymmetric stretching mode plays dominant roles in these dipole-forbidden transitions.

The perturbative approach proposed by Herzberg and Teller [14] provides a rational explanation of the findings. In this famous approach, the change in the Coulomb potential V due to molecular distortion is treated perturbatively and the electronic wave function at a geometry of $\boldsymbol{Q}_0 + \boldsymbol{Q}'$ is expressed as follows:

$$\Psi_s(\boldsymbol{r}_1, \cdots \boldsymbol{r}_N; \boldsymbol{Q}_0 + \boldsymbol{Q}') = \Psi_s(\boldsymbol{r}_1, \cdots \boldsymbol{r}_N; \boldsymbol{Q}_0) + \sum_{k \neq s,L} \frac{\langle \Psi_k | \frac{\partial V}{\partial Q_L} | \Psi_s \rangle}{E_s - E_k} \times \Psi_k(\boldsymbol{r}_1, \cdots \boldsymbol{r}_N; \boldsymbol{Q}_0) Q_L. \quad (11)$$

Here $\partial V/\partial Q_L$ represents the variation of the Coulomb potential due to a displacement from the reference geometry $\boldsymbol{Q}_0$ along the Lth normal coordinate. Equation (11) shows that changes in the atomic positions lead to the admixture of various electronic states in the zeroth-order term $\Psi_s(\boldsymbol{r}_1, \ldots, \boldsymbol{r}_N; \boldsymbol{Q}_0)$. It should be noted that such mixing effectively takes place only between states with a small energy separation due to the presence of the energy denominator $E_s - E_k$ in the perturbation correction. The influence of molecular distortion can therefore be neglected for the electronic ground state in a qualitative discussion, owing to its large separation in energy from other states. Consideration based on symmetry-point-group theory shows that the $1\,^1T_{1g}$ and $2\,^1T_{1g}$ excited states can couple to the close-lying $1\,^1T_{1u}$ state through the υ_3 vibration with the t_{1u} symmetry; the direct product group of $T_{1g} \times T_{1u} = A_{1u} + E_u + T_{1u} + T_{2u}$ involves a T_{1u} component and $\langle \Psi_{1\,^1T_{1u}} | \frac{\partial V}{\partial Q_{\upsilon_3}} | \Psi_{1\,^1T_{1g}} \rangle$ may thus have a nonzero value. As a consequence, the intensity borrowing from the $1\,^1T_{1u}$ transition takes place through the υ_3 vibration. It can be seen from Fig. 4 that the $1\,^1T_{1u}$ GOS profile has a dominant maximum at $K^2 = 0$. Thus, coupling with the $1\,^1T_{1u}$ dipole-allowed state leads to a substantial enhancement of the $1\,^1T_{1g}$ and $2\,^1T_{1g}$ transitions at small momentum transfer. Consideration of this kind gives a rational explanation why and how the $1\,^1T_{1g}$ and $2\,^1T_{1g}$ GOS profiles have much higher intensity than predicted by the equilibrium geometry calculation in the low-K^2 region.

V. CONCLUSION

In this paper we report an EELS study on the electronic excitations of SF_6. Angle-resolved EELS experiments have been carried out at incident electron energy of 3.0 keV and the GOS profiles of the low-lying transitions have been obtained from the electron-energy-loss spectra. Furthermore, theoretical calculations have been performed using a method of calculating GOS with vibrational effects being involved. It has been shown that taking into account vibrational effects brings significantly improved agreement with experiment for the $1\,^1T_{1g}$ transition. It has been elucidated that the coupling with the $1\,^1T_{1u}$ state via asymmetric SF stretching vibration plays important roles in the $1\,^1T_{1g}$ and $2\,^1T_{1g}$ dipole-forbidden transitions.

ACKNOWLEDGMENTS

This research was supported by the JSPS KAKENHI Grants No. 18H01932 and No. 25248002. It was also supported in part by the Management Expenses Grants for National Universities Corporation and the Cooperative Research Program of "NJRC Mater. & Dev."

[1] L. G. Christophorou and J. K. Olthoff, J. Phys. Chem. Ref. Data **29**, 267 (2000), and references therein.
[2] B. Goswami and B. Antony, RSC Adv. **4**, 30953 (2014), and references therein.
[3] J. L. Dehmer, J. Chem. Phys. **56**, 4496 (1972).
[4] J. T. Francis, C. C. Turci, T. Tyliszczak, G. G. B. de Souza, N. Kosugi, and A. P. Hitchcock, Phys. Rev. A **52**, 4665 (1995).
[5] K. Mitsuke, S. Suzuki, T. Imamura, and I. Koyano, J. Chem. Phys. **93**, 8717 (1990).
[6] D. Blechschmidt, R. Haensel, E. E. Koch, U. Nielsen, and T. Sagawa, Chem. Phys. Lett. **14**, 33 (1972).
[7] L. C. Lee, E. Phillips, and D. L. Judge, J. Chem. Phys. **67**, 1237 (1977).
[8] M. Sasanuma, E. Ishiguro, H. Masuko, Y. Morioka, and M. Nakamura, J. Phys. B: At. Mol. Opt. Phys. **11**, 3655 (1978).
[9] D. M. P. Holland, D. A. Shaw, A. Hopkirk, M. A. MacDonald, and S. M. McSweeney, J. Phys. B: At. Mol. Opt. Phys. **25**, 4823 (1992).
[10] A. P. Hitchcock and M. J. Van der Wiel, J. Phys. B: At. Mol. Phys. **12**, 2153 (1979).
[11] S. Trajmar and A. Chutjian, J. Phys. B: At. Mol. Phys. **10**, 2943 (1977).
[12] K. H. Sze and C. E. Brion, Chem. Phys. **140**, 439 (1990).
[13] P. J. Hay, J. Am. Chem. Soc. **99**, 1013 (1977).
[14] G. Herzberg and E. Teller, Z. Phys. Chem. B **21**, 410 (1933).
[15] M. Inokuti, Rev. Mod. Phys. **43**, 297 (1971).
[16] K. T. Leung, J. Electron Spectrosc. Relat. Phenom. **100**, 237 (1999).
[17] N. Watanabe, D. Suzuki, and M. Takahashi, J. Chem. Phys. **134**, 234309 (2011).
[18] N. Watanabe, T. Hirayama, D. Suzuki, and M. Takahashi, J. Chem. Phys. **138**, 184311 (2013).
[19] N. Watanabe and M. Takahashi, J. Phys. B: At. Mol. Opt. Phys. **47**, 155203 (2014).
[20] J. F. Ying, T. A. Daniels, C. P. Mathers, H. Zhu, and K. T. Leung, J. Chem. Phys. **99**, 3390 (1993).
[21] M. L. M. Rocco, C. A. Lucas, H. M. Boechat-Roberty, A. I. da Silva, Jr., and G. G. B. de Souza, J. Braz. Chem. Soc. **9**, 287 (1998).
[22] M. Takahashi, N. Watanabe, Y. Wada, S. Tsuchizawa, T. Hirosue, H. Hayashi, and Y. Udagawa, J. Electron Spectrosc. Relat. Phenom. **112**, 107 (2000).
[23] M. Inokuti, J. L. Dehmer, T. Baer, and J. D. Hanson, Phys. Rev. A **23**, 95 (1981), and references therein.
[24] N. Watanabe, M. Yamazaki, and M. Takahashi, J. Chem. Phys. **137**, 114301 (2012).
[25] N. Watanabe, M. Yamazaki, and M. Takahashi, J. Chem. Phys. **141**, 244314 (2014).
[26] N. Watanabe, M. Yamazaki, and M. Takahashi, J. Electron Spectrosc. Relat. Phenom. **209**, 78 (2016).
[27] T. H. Dunning, Jr., J. Chem. Phys. **90**, 1007 (1989).
[28] R. A. Kendall, T. H. Dunning, and R. J. Harrisson, J. Chem. Phys. **96**, 6796 (1992).
[29] M. W. Schmidt, K. K. Baldridge, J. A. Boatz, S. T. Elbert, M. S. Gordon, J. H. Jensen, S. Koseki, N. Matsunaga, K. A. Nguyen, S. J. Su, T. L. Windus, M. Dupuis, and J. A. Montgomery, J. Comput. Chem. **14**, 1347 (1993).
[30] C. Chapados and G. Birnbaum, J. Mol. Spectrosc. **132**, 323 (1988).
[31] J. F. Stanton and R. J. Bartlett, J. Chem. Phys. **98**, 7029 (1993).
[32] T. H. Dunning, Jr., K. A. Peterson, and A. K. Wilson, J. Chem. Phys. **114**, 9244 (2001).

[33] N. Watanabe, D. Suzuki, and M. Takahashi, J. Chem. Phys. **134**, 064307 (2011).
[34] N. Watanabe, H. Hayashi, Y. Udagawa, S. Ten-no, and S. Iwata, J. Chem. Phys. **108**, 4545 (1998).
[35] N. Watanabe, S. Ten-no, S. Iwata, and Y. Udagawa, in *Review of Modern Quantum Chemistry*, edited by K. D. Sen (World Scientific, Singapore, 2002), p. 553.
[36] C. Winstead and V. McKoy, J. Chem. Phys. **121**, 5828 (2004).
[37] A. Dreuw and M. Head-Gordon, Chem. Rev. **105**, 4009 (2005).
[38] Y. Zhao and D. G. Truhlar, Theor. Chem. Acc. **120**, 215 (2008).
[39] A. Kumar, G. R. G. Fairley, and W. J. Meath, J. Chem. Phys. **83**, 70 (1985).